

# Solc filters in a reflective geometry

Abdelghafour Messaadi<sup>1</sup>, Asticio Vargas<sup>2</sup>, María M. Sánchez-López<sup>3</sup>,  
Pascuala García-Martínez<sup>4</sup>, Przemysław Kula<sup>5</sup>, Noureddine Bennis<sup>5</sup> and  
Ignacio Moreno<sup>1,\*</sup>

<sup>1</sup>Departamento de Ciencia de Materiales, Óptica y Tecnología Electrónica, Universidad Miguel Hernández, 03202 Elche, Spain

<sup>2</sup>Departamento de Ciencias Físicas, Universidad de La Frontera, Temuco, Chile

<sup>3</sup>Instituto de Bioingeniería, Departamento de Física y Arquitectura de Computadores, Universidad Miguel Hernández, 03202 Elche, Spain

<sup>4</sup>Departament d'Òptica, Universitat de València, 46100 Burjassot, Spain

<sup>5</sup>Military University of Technology, Kaliskiego 2 St., 00-908 Warsaw, Poland

\*Corresponding author: [i.moreno@umh.es](mailto:i.moreno@umh.es)

## Abstract

We present the realization of a bulk optics birefringent Solc filter in a reflective geometry. This geometry reduces by half the number of required retarders, ensures the same spectral retardance function in pairs of retarders, and helps to make more compact filters. The key element is a quarter-wave Fresnel rhomb located in between the set of retarders and a mirror. Two cases are considered: the first Solc filter uses multiple-order quartz retarders, and the second one uses two liquid-crystal retarders. The latter has the advantage of being tunable via an applied voltage. Experimental results show how to filter the spectral content of a supercontinuum laser.

**Keywords:** Birefringence; Polarization; Spectral Filters; Liquid-crystal devices.

## 1. INTRODUCTION

Solc filters [1,2] are classical birefringent filters composed of a stack of identical retardation elements with orientations defined according to the number of retarders included in the filter. There are two classes [3]: a) folded Solc filters, where the set of retarders has the same, but alternating orientation and is sandwiched between crossed polarizers, and b) fan Solc filters, where the retarders orientation progressively increases

in a fixed angle and the set of plates is sandwiched between parallel polarizers. They can be generated either with bulk optical retarder elements or with fiber optics components [4]. Their wavelength-filtering characteristics are based on changing the state of polarization of light through the spectral retardance of the birefringent plates, which is given by  $\phi = k\Delta n \cdot d$ , where  $k = 2\pi/\lambda = 2\pi f/c$  is the wavenumber ( $f$  denotes the frequency,  $\lambda$  the wavelength and  $c$  the speed of light),  $\Delta n = n_e - n_o$  is the birefringence of the anisotropic material ( $n_e$  and  $n_o$  are the extraordinary and ordinary refractive indices), and  $d$  is the thickness of the plate or the length of the fiber.

Therefore, considering the relative orientation of the input and output polarizers, the retardance achieves the condition for maximum transmission only at certain wavelengths and the Solc filter acts as a selective spectral filter. For instance, the spectral maxima in folded Solc filters occur at wavelengths where the retardance equals an odd integer number of  $\pi$  radians, i.e., whenever the plates are half-wave retarders (HWR) [3]. The free spectral range (FSR), i.e., the separation between two consecutive maxima, is fixed by the plates and, when expressed in frequencies, is given by  $FSR = \Delta f = c/\Delta n \cdot d$ . The width of these transmission peaks is reduced as the number of retarders composing the filter increases.

Despite being classical long established designs, Solc filters continue to be very useful elements. Recent studies include their low-cost production by using commercial cellophane tape [5], the generation of fast tunable filters by employing electro-optic retarders [6], which can be integrated in a waveguide [7,8], their combination with other filters to generate tunable narrow-band filters [9], or their realization with polarizing maintaining fibers, in order to build optical fiber sensors [10,11]. And other related birefringent filter designs have been theoretically demonstrated [12-14].

In all cases, a crucial aspect for the success in the realization of the filter is that all the retarders must exhibit the same spectral retardance function. Otherwise, the retardance mismatch for the design wavelength prevents the maximum transmission of the filter. This is why all the plates composing the filter must be made of the same material; but even then small differences in the retarder thickness (or length, if it is a fiber) results in the failing operation of the filter.

In this paper we demonstrate the experimental realization of a bulk optics Solc filter generated in a reflective geometry. This geometry presents advantages since the same retarders are used twice, thus doubling the effective number of retarders in the filter and ensuring the same spectral retardance function. A reflective geometry was proposed for Lyot filters in Ref. [15]. And a reflective geometry for Solc type filters was proposed previously in Ref. [13], although its experimental realization was not reported. The key element in our experimental system is a Fresnel rhomb quarter-wave retarder (FR-QWR) placed in between the mirror and the set of retarders. The combination of a QWR and the mirror acts as a special element sometimes called a polarization conversion mirror (PCM) [16], which has demonstrated to be useful for the realization of polarization-independent tunable filters [17]. Our novel proposal of using an FR-QWR allows producing such PCM, but in a very wide spectral range. This way it is possible to generate a reflective Solc filter that uses the same series of retarders directly in a double-pass geometry.

After this introduction, the paper is organized as follows: Section 2 presents the description of the optical system and its mathematical treatment. Then, Section 3 presents the experimental system and experimental data for two different Solc filters, one based on multiple-order quartz retarders, and the other based on tunable liquid-crystal retarders. Finally, Section 4 contains the conclusions of our work.

## 2. OPTICAL SYSTEM

Figure 1 shows a scheme of the optical system. It consists in a beam-splitter, a chain of retarders, and a mirror. The figure illustrates a folded Solc filter, with only a single couple of retarders, the first with orientation  $+\rho$  and the second with orientation  $-\rho$ . The beam-splitter ideally could be a polarizing beam-splitter (PBS). In our case, however, since a PBS covering the entire experimental spectral range was not available, we selected a non-polarizing beam-splitter (NPBS) and employed two linear polarizers at the input (LP1) and output (LP2). Finally, a FR-QWR was placed in between the set of retarders and the mirror. The input and output reference frameworks are indicated in the figure. And the  $s$  and  $p$  polarization components are parallel to the  $x$  (vertical laboratory axis) and  $y$  (horizontal laboratory axis) directions.

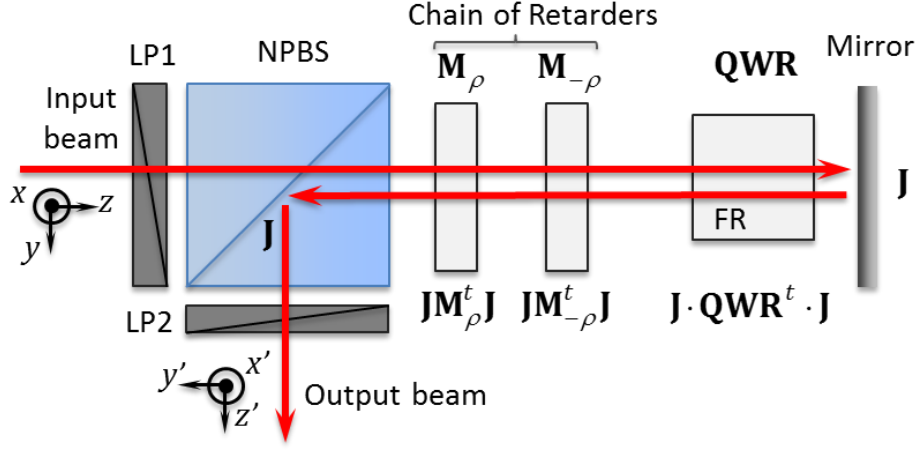


Fig. 1. Optical system. NPBS: non-polarizing beam splitter; LP: linear polarizers; FR: Fresnel rhomb quarter-wave retarder.

In order to mathematically describe the system, we follow the Jones matrix formalism, adapted to reflective polarization devices as presented in Ref. [18]. This formulation allows not only the physical explanation of the system, but also the numerical calculation of the filter's transmission. Following this formalism, if  $\mathbf{M}_r$  denotes the usual Jones matrix of a given retarder operating in transmission, the same retarder operating in the backward passage after a reflection is described by the Jones matrix product  $\mathbf{J}\mathbf{M}_r^t\mathbf{J}$  where  $\mathbf{J} = \text{diag}(+1, -1)$ , and  $t$  denotes the transposed matrix [16]. The linear retarder Jones matrix is given by  $\mathbf{M}_r = \mathbf{R}(-r)\mathbf{M}_0\mathbf{R}(+r)$ , where  $\mathbf{M}_0 = \text{diag}(1, \exp(ir))$ ,  $\phi$  is the retardance and  $\mathbf{R}(\rho)$  the  $2 \times 2$  rotation matrix. The mirror and the ideal NPBS are described within this formalism with a  $\mathbf{J}$  matrix.

For the sake of clarity, Fig. 1 shows the Jones matrices of the optical elements: in the upper arrow, those related to the forward passage of light through the birefringent elements; and in the bottom arrow those corresponding to the backward passage. Therefore, the Jones matrix sequence for the reflective system in Fig. 1, when the FR-QWR is absent, is given by the following Jones matrix product:

$$\mathbf{M}_{ref} = \mathbf{J} \cdot (\mathbf{J}\mathbf{M}_{+\rho}^t\mathbf{J}) \cdot (\mathbf{J}\mathbf{M}_{-\rho}^t\mathbf{J}) \cdot \mathbf{J} \cdot \mathbf{M}_{-\rho} \cdot \mathbf{M}_{+\rho}. \quad (1)$$

This matrix accounts for the system of retarders (the two linear polarizers in Fig. 1 are not included). Taking into account that  $\mathbf{M}_r^t = \mathbf{M}_r$  and  $\mathbf{J}^2 = \mathbf{I}$  (the identity matrix), the above equation simplifies to:

$$\mathbf{M}_{ref} = \mathbf{M}_{+\rho} \cdot \mathbf{M}_{-\rho} \cdot \mathbf{M}_{-\rho} \cdot \mathbf{M}_{+\rho} \cdot \quad (2)$$

Note that this is not the correct sequence for the folded Solc filter, since the two last retarders have the opposite orientation.

The solution to this issue is the use of a PCM [16]. In our case, we require a wavelength-independent PCM that works in a wide operating spectral range. This is why we use a FR-QWR. Fresnel rhombs are retarders with almost wavelength independent retardance, since their retardance is not based on birefringence but on the phase difference upon total internal reflection between the *s* and *p* polarization components [19]. The FR-QWR is placed behind the set of retarders composing the Solc filter and before the mirror (Fig. 1). Since light passes twice through the rhomb, it therefore acts as a HWR for all wavelengths. This HWR induces the polarization transformation required to produce the folded Solc filter geometry. The combination of the rhomb and the mirror produces a wavelength-independent PCM.

Therefore, the introduction of the FR-QWR in the system modifies Eq. (1) as follows:

$$\mathbf{M}_{ref} = \mathbf{J} \cdot (\mathbf{J}\mathbf{M}_{+\rho}^t\mathbf{J}) \cdot (\mathbf{J}\mathbf{M}_{-\rho}^t\mathbf{J}) \cdot (\mathbf{J} \cdot \mathbf{QWR}^t \cdot \mathbf{J}) \cdot \mathbf{J} \cdot \mathbf{QWR} \cdot \mathbf{M}_{-\rho} \cdot \mathbf{M}_{+\rho}, \quad (3)$$

where  $\mathbf{QWR} = \text{diag}(1, i)$  stands for the aligned quarter-wave retarder. Thus, taking into account that  $\mathbf{J} \cdot \mathbf{QWR}^t \cdot \mathbf{J} = \mathbf{QWR}$ , and  $\mathbf{QWR} \cdot \mathbf{J} \cdot \mathbf{QWR} = \mathbf{I}$ , Eq. (3) can be simplified as

$$\mathbf{M}_{ref} = \mathbf{J} \cdot (\mathbf{J}\mathbf{M}_{+\rho}^t\mathbf{J}) \cdot (\mathbf{J}\mathbf{M}_{-\rho}^t\mathbf{J}) \cdot \mathbf{M}_{-\rho} \cdot \mathbf{M}_{+\rho}, \quad (4)$$

Finally, this sequence can be further simplified taking into account again that  $\mathbf{J}\mathbf{M}_{r}^t\mathbf{J} = \mathbf{M}_{-r}$ , and the result is now:

$$\mathbf{M}_{ref} = \mathbf{J} \cdot \mathbf{M}_{-\rho} \cdot \mathbf{M}_{+\rho} \cdot \mathbf{M}_{-\rho} \cdot \mathbf{M}_{+\rho} \cdot \quad (5)$$

Notice that now the orientation angle of the retarders alternates the sign in a correct sequence. The final  $\mathbf{J}$  matrix in Eq. (5), which corresponds to the reflection at the NPBS, acts as a HWR oriented at zero degrees, which could be compensated with a HWR Fresnel rhomb retarder. However, since the Solc filter operates with a final polarizer aligned with this retarder, this compensation is not necessary to achieve the same intensity transmission.

We note that the role of the FR-QWR element in our bulk optics filter can be regarded the role of a circulator-loop in a fiber optic birefringent filter [20].

### **3. EXPERIMENTAL RESULTS**

#### **3.1. Experimental system**

Let us now describe the experimental system and show the effect of the FR-QWR as mirror compensator. A supercontinuum laser from Fianium, model SC400 is used as the light source. We use two Glan-Taylor polarizing cubes from Edmund Optics that exhibit good extinction ratio in a wide spectral range, and a NPBS from Thorlabs, model BS013, which was verified to not introduce additional polarization or spectral effects. Finally, the output beam is captured with a STN-F600-UVVIS-SR optical fiber connected to a VIS spectrometer from Stellar-Net, STN-BLK-C-SR, which measures the spectrum from 200 nm to 1080 nm.

Figure 2(a) shows the result of a first experiment that verifies the actuation of the FR-QWR in the system. The two polarizers were set parallel, both oriented at  $45^\circ$  with respect to the vertical laboratory framework. No set of retarders was included in the optical system. The blue curve shows the spectrum captured with the spectrometer. We select the spectral range in between 500 nm and 800 nm, where there is enough light emission from the laser and the NPBS works properly. The results are given directly in counts of the spectrometer. The captured spectrum basically reproduces the supercontinuum laser emission spectrum. Note that the input light beam is reflected back with the same polarization and therefore it is fully transmitted by LP2.

Next the FR-QWR is introduced in the system, with the principal axis oriented at zero, in order to generate the PCM for all wavelengths. We used a FR-QWR from Thorlabs, model FR600QM. We verified a transmission of more than 93% of the laser light intensity when passing through the rhomb. Now the spectrum in Fig. 2(a) (red curve) is zero for all wavelengths. Note that a retardance dispersion in the QWR would prevent the realization of this broadband transformation.

#### **3.2. Solc filter with quartz retarders**

For the next experiment we use two identical multiple-order quartz plates, designed as QWRs for the wavelength of 633 nm. Multiple-order plates exhibit large retardance dispersion that can be exploited in birefringent filters [21]. In order to calibrate their spectral retardance, we

introduced them in the system. Figure 2(b) shows the spectrum measured with the same system settings (LP1 and LP2 both oriented at  $45^\circ$ , and FR-QWR oriented at zero).

But now one of the quartz retarders is placed in between the NPBS and the FR-QWR. The quartz retarder is also oriented at zero. In this situation, the transmission of the system is given by [22,23]:

$$T(\lambda) \propto \cos^2\left[\frac{1}{2}(2\phi(\lambda) + \pi)\right]. \quad (6)$$

where  $\phi(\lambda)$  is the spectral retardance of the quartz retarder (the factor 2 is due to the double pass through the retarder, and the additional  $\pi$  term is the retardance due to the FR-QWR). Since the retardance of the multiple-order retarder varies rapidly with wavelength, typically as  $\phi = k\Delta n \cdot d$ , the spectrum in Fig. 2(b) displays the characteristic oscillatory pattern [24]. We verified that the second quartz retarder exhibits equivalent oscillatory spectrum, thus providing identical spectral retardance.

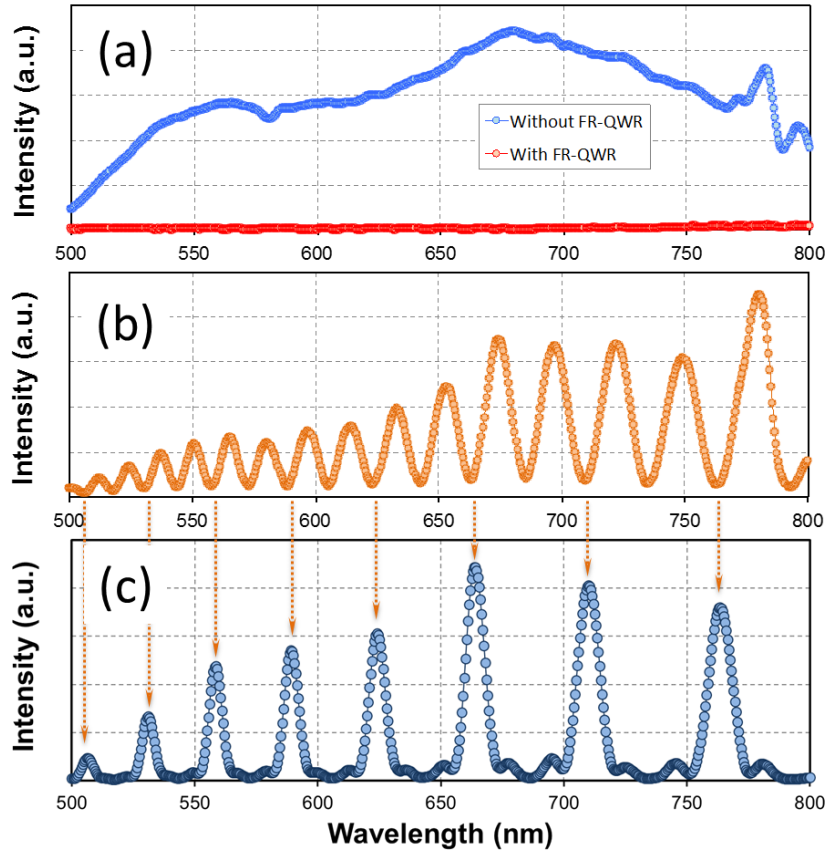


Fig. 2. (a,b) Spectral intensity  $T(\lambda)$  measured with LP1 and LP2 oriented at  $+45^\circ$ . (a) Without any retarders-chain, with and without FR-QWR. (b) With one quartz multiple-order retarder and the FR-QWR. (c) Spectral intensity for the Solc filter with  $N=4$  using just two retarders.

Note that whenever the plate retardance reaches an integer number of  $\pi$  radians a minimum of the transmission curve  $T(\lambda)$  in Fig. 2(b) is obtained. The condition for a maximum transmission in the Solc filter is half-wave retardance. Thus, when these plates are used to build such a folded Solc filter, the maxima should be located at these wavelengths where the minima in Fig. 2(b) are observed, but only in every other minimum. The arrows in bottom of Fig. 2(b) indicate the minima corresponding to retardances that are odd integers of  $\pi$  radians. These values are verified in Fig. 2(c), where the folded Solc filter is generated. In this case, the two polarizers were oriented at  $0^\circ$  and  $90^\circ$ , respectively. The orientation of each retarder element in the folded Solc filter [3] is given by  $\vartheta_n = (-1)^n \rho$  with  $n=1,2,\dots, N$  number of elements, and

$$\rho = \frac{\pi}{4N}. \quad (7)$$

Since we have two plates, the reflective geometry allows a Solc filter with  $N=4$  elements, and the angle is  $\rho=11.25^\circ$ . The captured spectrum in Fig. 2(c) shows the characteristic profile of the Solc filter. Note how the wavelengths where the maxima are located correspond to one out of two minima of the curve in Fig. 2(b). Also note the side-lobes characteristic of the Solc filter transmission.

### 3.3. Tunable Solc filter with liquid-crystal retarders

Once the reflective geometry was demonstrated, we were interested in making the Solc filter tunable. Therefore, tunable linear retarders were required. Liquid-crystal retarders (LCR) [27] are one very useful option. They have been used in a number of spectral birefringent filters, including tunable Lyot filters [25], or dynamic colour filters that combine cholesteric liquid crystal layers [26].

We used LCR fabricated at the Military University of Technology of Warsaw. They are two parallel-aligned nematic LCR devices that were prepared with polished Indium Tin Oxide (ITO) coated glass plates. Homogeneous planar alignment was induced on ITO by spin-coated polyimide SE-130 (from NISSAN Chemical Industries) followed by curing and antiparallel rubbing process steps. The thickness of the cells was kept about  $5 \mu\text{m}$ . The cells were filled with Mix-3 high birefringent liquid-crystal material to produce a wide tuning range of the filter [28]. The effective retardance can be varied via an applied

voltage. A DC balanced square voltage signal of 1 kHz was applied, and the peak-to-peak voltage ( $V_{pp}$ ) controls the retardance, the greater  $V_{pp}$  the lower the retardance. Figure 3 shows a picture of the optical system with the two LCRs. Note that they have been mounted onto rotatable mounts, and also note the inclusion of two iris diaphragms to help aligning the laser. The supercontinuum laser is kept with relatively low intensity, to avoid any possible damage of the devices. However, note that if high-power lasers were required, other alternatives could be used such as polycrystalline liquid crystal retarders [29].

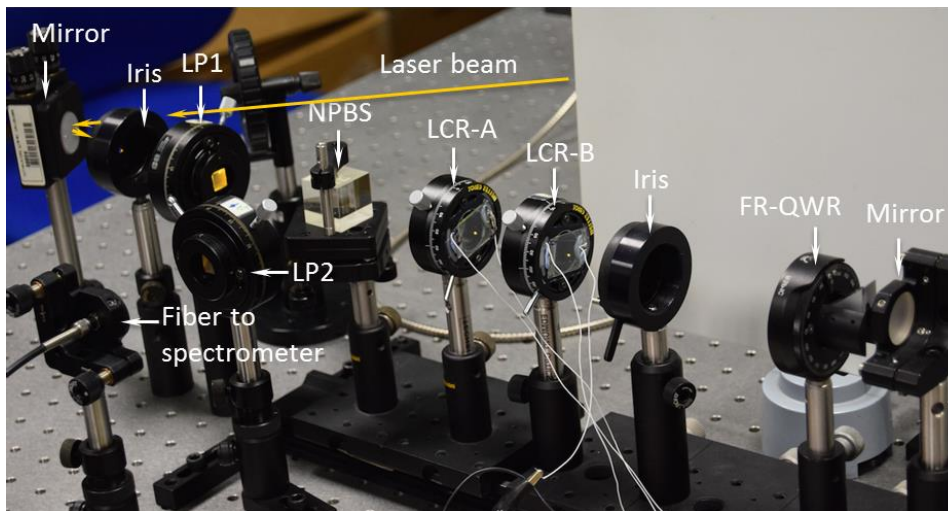


Fig. 3. Picture of the optical system for the Solc filter with two LCRs.

We repeated the experiment described in Fig. 2(b) to calibrate the retardance of these two LCR devices without applied voltage. The devices were labeled as LCR-A and LCR-B. The results are shown in Fig. 4(a), where the retardance is indicated at some specific minima. These values were deduced by counting the minima that were observed in the curve as we increase the voltage [30]. Note the high retardance values obtained thanks to the use of a high birefringent liquid crystal ( $\Delta n$  is approximately 0.46 for 650 nm) [28]. The curves in Fig. 4(a), although very similar, show that the retardance is not exactly the same for the two LCRs, probably due to a small difference in the LC layer thickness. This can be a major problem in the realization of a Solc filter. Fortunately, we can control the applied voltage to adjust the curves to reach the minima and maxima at the same wavelengths in order to provide the same spectral retardance in both LCRs. The reflective geometry helps to alleviate this problem: the same retardance is ensured

in pairs of elements, since it is the same retarder that plays twice. The result in Fig. 4(a) indicates that the retardance of LCR-A is slightly greater than that of LCR-B.

Therefore, a small voltage applied to LCR-A compensates for this extra retardance. As indicated in Fig. 4(a), increasing the  $V_{pp}$  applied to the LCRs moves the spectral oscillations to lower wavelengths, since the retardance is reduced.

Figures 4(b), 4(c) and 4(d) show the spectral transmission of the Solc filter for different couples of voltages applied to each LCR. Again, since we use two retarders, we have  $N=4$  and the rotation angle is  $\rho=11.25^\circ$ . In Fig. 4(b) voltage is only applied to LCR-A to match the retardance of LCR-B. The transmission peaks of the filter are centered at 550 nm and 640, i.e. the FSR is 90 nm in this region. The FWHM at these two bands are 15 and 30 nm respectively. These peaks correspond to retardances  $9\pi$  and  $7\pi$  respectively in Fig. 4(a). The figure also includes a simulation of the Solc filter's transmittance based on the spectral retardance deduced from the data in Fig. 4(a), showing very good agreement with the experimental transmission.

In Fig. 4(c) the voltage is increased in both devices, in order to shift these retardance values to the wavelength in between:  $7\pi$  at approximately 585 nm and  $9\pi$  at approximately 515 nm. Therefore, now the peaks of the Solc filter are shifted to these wavelengths. Note that another peak enters the experimental spectral range from the right, corresponding to a retardance of  $5\pi$  and yields another maximum at approximately 740 nm.

Finally, in Fig. 4(d), the voltages applied to each LCR are augmented further in order to locate a maximum again at 550 nm, now corresponding to a retardance of  $7\pi$ . Note how, because the voltages are greater and therefore  $\Delta n$  is lower, the next maxima to the right (corresponding to a retardance of  $5\pi$ ) is located at approximately 680 nm, thus providing a much larger FSR than the case in Fig. 4(b). Simulation results agree quite well with the experiments in all cases. These results thus confirm the effective realization of a tunable Solc filter in a reflective geometry.

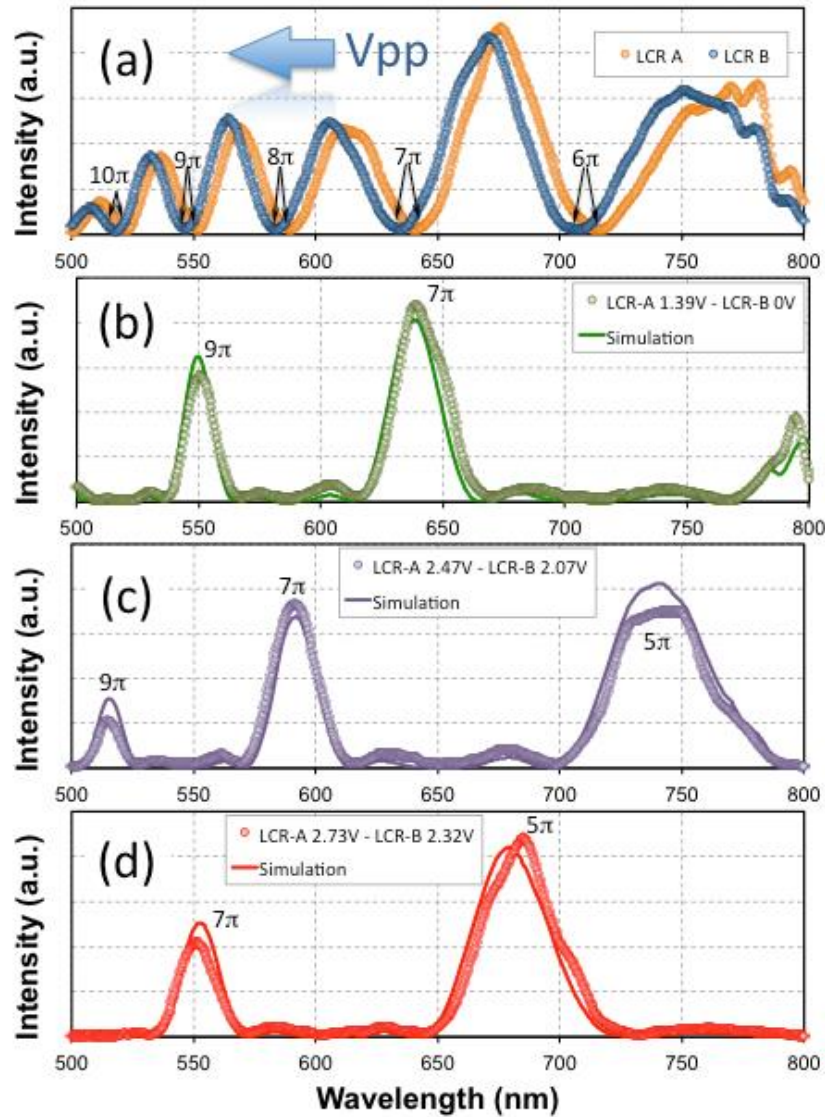


Fig. 4. (a) Spectral intensity measured with LP1 and LP2 oriented at  $+45^\circ$  for LCR-A and LCR-B without applied voltage. And spectral intensity of the Solc filter with  $N=4$  using two retarders with different voltages: (b) LCR-A 1.39V, LCR-B 0V; (c) LCR-A 2.47V, LCR-B 2.07V; (d) LCR-A 2.73V, LCR-B 2.32V. The value of the retardance of each LCR is indicated at the maxima of the Solc filters.

#### 4. CONCLUSIONS

In summary, a bulk optics birefringent Solc filter that operates in a reflective geometry was experimentally demonstrated. This reflective geometry relies on the inclusion of a wavelength independent FR-QWR. The FR-QWR-mirror combination allows the reflective Solc filter geometry in a wide spectral range. Since light passes twice through each retarder in the filter set, the effective number of retarders is doubled and the same spectral retardance function is ensured in pairs of elements.

We experimentally demonstrated the proposed system with static quartz plates, and also with tunable liquid-crystal retarders. We used the system to filter a supercontinuum laser source. In both cases we reproduced the characteristic spectral transmission of the Solc filter, and in the second case we were able to tune the transmission function.

We expect that this geometry, which was demonstrated here with bulk optics, can also be implemented in compact integrated Solc filters and with other related birefringent filter designs.

### **Acknowledgements**

M. M. Sánchez-López, P. García-Martínez and I. Moreno acknowledge support from Ministerio de Economía y Competitividad of Spain and FEDER funds (grant ref.: FIS2015-66328-C3-3-R). A. Vargas acknowledges support from Fondecyt (grant ref.: 1151290). N. Bennis and P. Kula acknowledge the Polish Ministry of Science and Higher Education the Statutory Activity PBS-654 and PBS-651 of Military University of Technology respectively.

### **References**

- [1]. J. W. Evans, "Solc birefringent filter", *J. Opt. Soc. Am.* **48**, 142-145 (1958).
- [2]. I. Solc, "Birefringent chain filters", *J. Soc. Opt. Am.* **55**, 621-625 (1965).
- [3]. P. Yeh, "Some applications of anisotropic layered media", Ch. 10 in *Optical Waves in Layered Media*, John Wiley & Sons (2005). ISBN 0-471-73192-7.
- [4]. M. Johnson, "Single-mode-fiber birefringent filters", *Opt. Lett.* **5**, 142-145 (1980).
- [5]. P. Velásquez, M. M. Sánchez-López, I. Moreno, D. Puerto, F. Mateos, "Interference birefringent filters fabricated with low cost commercial polymers", *Am. J. Phys.* **73**, 357-361 (2005).
- [6]. X. Chen, J. Shi, Y. Chen, Y. Zhu, Y. Xia, Y. Chen, "Electro-optic Solc-type wavelength filter in periodically poled lithium niobate", *Opt. Lett.* **28**, 2115-2117 (2003).

- [7]. Y. L. Lee, N. E. Yu, C.-S. Kee, D.-K. Ko, J. Lee, B.-A. Yu, W. Shin, T. J. Eom, Y.-C. Noh, "Wavelength filtering characteristics of Solc filter based on Ti:PPLN channel waveguide", *Opt. Lett.* **32**, 2813-2815 (2007).
- [8]. Q. Zhang, X. Zeng, F. Pang, X. Chen, T. Wang, "Tunable polarization-independent Solc-type wavelength filter based on periodically poled lithium niobate", *Opt. Laser Technol.* **44**, 1992-1994 (2012).
- [9]. M. Abuleil, I. Abdulhalim, "Narrowband multispectral liquid crystal tunable filter", *Opt. Lett.* **41**, 1957 (2016).
- [10]. R. H. Chu, J. J. Zou, "Transverse strain sensing based on optical fibre Solc filter", *Opt. Fiber. Technol.* **16**, 151-155 (2010).
- [11]. S. Jo, Y. Kim, Y. W. Lee, "Study on transmission and output polarization characteristics of a first-order Lyot-type fiber comb filter using polarization-diversity loop", *IEEE Photonics J.* **7**, 7801015 (2015).
- [12]. Q. Wang, G. Farrell, Y. Semenova, "Optimal design of birefringent filter with a flat-top passband", *J. Opt. A: Pure Appl. Opt.* **8**, 652-656 (2006).
- [13]. G. Shabtay, E. Eidinge, Z. Zalevsky, D. Mendlovic, E. Marom, "Tunable birefringent filters – optimal iterative design", *Opt. Express* **10**, 1534-1541 (2002).
- [14]. A. R. Halassi, R. Hamdi, D. F. Bendimerad, B.-E. Benkelfat, "A novel synthesis approach for birefringent filters having arbitrarily amplitude transmittances", *Opt. Commun.* **369**, 12-17 (2016).
- [15]. D. F. Bendimerad, B.-E. Benkelfat, Y. Gottesman, O. Seddiki, B. Vinouze, R. Hamdi, "Contrast and finesse enhancement in a birefringent filter", *IEEE Photonics Technol. Lett.* **23**, 1721-1723 (2011).
- [16]. I. Abdulhalim, "Polarization independent birefringent tunable filters", US patent US 8,369,014 B2 (2013).
- [17]. I. Abdulhalim, "Polarization independent birefringent Fabry-Perot etalon having polarization conversion mirrors", *Opt. Commun.* **282**, 3052-3054 (2009)

- [18]. C. R. Fernández-Pousa, I. Moreno, N. Bennis, and C. Gómez-Reino, "Generalized formulation and symmetry properties of anisotropic devices: Application to liquid crystal displays", *J. Opt. Soc. Am. A* **17**, 2074–2080 (2000).
- [19]. D. Mawet, C. Hanot, C. Leunerts, P. Riaud, D. Defrére, D. Vandormael, J. Loicq, K. Fleury, J. Y. Plessier, J. Surdej, S. Habraken, "Fresnel rhombs as achromatic phase shifters for infrared nulling interferometry", *Opt. Express* **15**, 12850- 12865 (2007).
- [20]. J. Ge, H. Feng, G. Scott, M. P. Fok, "High-speed tunable microwave photonic notch filter based on phase modulator incorporated Lyot filter", *Opt. Lett.* **40**, 48-51 (2015).
- [21]. N. N. Nagib, S. A. Khodier, H. M. Sidki, "Retardation characteristics and birefringence of a multiple-order crystalline quartz plate", *Opt. Laser Technol.* **35**, 99-103 (2003).
- [22]. S.-T. Wu, U. Efron, L. D. Hess, "Birefringence measurements of liquid crystals", *Appl. Opt.* **23**, 3911-3915 (1984).
- [23]. A. Safrani, I. Abdulhalim, "Spectropolarimetric method for optic axis, retardation, and birefringence dispersion measurement", *Opt. Eng.* **48**, 053601 (2009).
- [24]. A. Messaadi, M. Mar Sánchez-López, P. García-Martínez, A. Vargas, I. Moreno, "Optical system for measuring the spectral retardance function in an extended range", *J. Eur. Opt. Soc. – Rapid. Pub.* **12**, 12:21 (2016).
- [25]. J. Beeckman, T. Hui, P. J. M. Vanbrabant, R. Zmijan, K. Neyts, "Polarization selective wavelength tunable filter", *Mol. Cryst. Liq. Cryst.* **502**, 19-28 (2009).
- [26]. H. Chen, R. Zhu, Y.-H. Lee, S.-T. Wu, "Correlated color temperature tunable white LED with a dynamic color filter", *Opt. Express* **24**, A731-A739 (2016).
- [27]. A. Peinado, A. Lizana, J. Campos, "Design of polarimeters based on liquid crystals and biaxial crystals for polarization metrology", *Opt. Pura Apl.* **49**, 167-177 (2016).
- [28]. D. Venkata Sai, P. Sathyanarayana, V.S.S. Sastry, J. Herman, P. Kula, R. Dabrowski, S. Dhara, "Birefringence, permittivity, elasticity and rotational viscosity of ambient temperature, high birefringent nematic liquid crystal mixtures", *Liquid Crystals* **41**, 591 (2014).
- [29]. L. De Sio, N.V. Tabyrian, R. Caputo, A. Veltri, C. Umeton, "POLICRYPS structures as switchable optical phase modulators", *Opt. Express* **16**, 7619-7624 (2008).

- [30]. A. Vargas, R. Donoso, M. Ramírez, J. Carrión, M. M. Sánchez-López, I. Moreno, "Liquid crystal retarder spectral retardance characterization based on a Cauchy dispersion relation and a voltage transfer function", *Opt. Rev.* **20**, 378-384 (2013).